Multi-dimensional two-phase flow modeling applied to interior ballistics

Julien Nussbaum, Philippe Helluy, Jean-Marc Hérard, Barbara Baschung

J_ID: AMJ DOI: 10.1115/1.4004293 Date: 7-June-11 Stage: Page: 1 Total Pages: 10

Multi-Dimensional Two-Phase Flow Modelling Applied to Interior Ballistics

Julien Nussbaum
ISL - French-German Research Institute of Saint-Louis,
5 rue du Général Cassagnou, BP 70034,
68301 Saint-Louis Cedex, France
e-mail: julien.nussbaum@isl.eu

Philippe Helluy
IRMA, Université de Strasbourg,
7 rue Descartes,
67084 Strasbourg Cedex,
e-mail: helluy@math.unistra.fr

Jean-Marc Herard
EDF, Research Branch,
MFEE, 6 quai Watier,
78400 Chatou, France
e-mail: jean-marc.herard@edf.fr

Barbara Baschung
ISL - French-German Research Institute of Saint-Louis,
5 rue du Général Cassagnou, BP 70034,
68301 Saint-Louis Cedex, France
e-mail: barbara.baschung@isl.eu

Complex phenomena occur in a combustion chamber during a ballistic cycle. From the ignition of the black powder in the primer to the exit of the projectile through the muzzle, two-phase gas-powder mix undertakes various transfers in different forms. A detailed comprehension of these effects is fundamental to predict the behavior of the whole system, considering performances and safety. Although the ignition of the powder bed is three-dimensional due to the primer's geometry, simulations generally only deal with one- or two-dimensional problem. In this study, we propose a method to simulate the two-phase flows in 1, 2 or 3 dimensions with the same system of partial differential equations. A one-pressure, conditionally hyperbolic model [1] was used and solved by a nonconservative finite volume scheme associated to a fractional step method, where each step is hyperbolic. We extend our study to a two-pressure, unconditionally hyperbolic model [2] in which a relaxation technique was applied in order to recover the one-pressure model by using the granular stress. The second goal of this study is also to propose an improved ignition model of the powder grains, by taking into account simplified chemical kinetics for decomposition reactions in the two phases. Here we consider a 0^{th}-order solid decomposition and an unimolecular, 2^{nd}-order gas reaction. Validation of the algorithm on several test cases is presented. [DOI: 10.1115/1.4004293]

Keywords: interior ballistics, ignition, combustion, two-phase flow, finite volume method

1 Introduction to the Problem

The geometry of a gun can be modeled by a cylinder with a variable cross section which represents the combustion chamber and the lunching tube. On the axis of the combustion chamber, at the breech, is placed the primer, a cylinder perforated by several holes on its circumference and filled with black powder. The space defined by the combustion chamber is partly filled with propellant. At initial time, the rear flat face of the projectile corresponds to the junction between the cone and the lunching tube (see Fig. 1 for an example of initial configuration).

At firing, the black powder is ignited by a mechanical or electrical system. The very fast combustion of the black powder produces hot gases that escape from the primer through the holes and spread through the propellant bed, producing the progressive ignition of the grains. The combustion of the propulsive powder produces a large amount of hot gases, increasing the pressure in the combustion chamber. When the pressure is sufficiently high, the projectile is accelerated by the expansion of the hot gases to the muzzle of the exit tube.

The propagation of the grains' ignition leads to the development of pressure waves. These waves have a great influence on the good functioning of the lunching system. Therefore, they have to be correctly modeled. In this study, we want to highlight two weaknesses of common simulators. First, the two-phase flows are naturally three dimensional, because the distribution of holes on the primer's surface is not axisymmetric. The flows can be approximated by one- or two-dimensional equations, but the front flame development in the powder bed (and thus the pressure waves) is better fitted with three-dimensional equations. Secondly, the ignition criterion for the grains is generally very inaccurate: one considers that a grain starts to burn when its surface temperature reaches an experimentally determined temperature. But these experimental conditions are far from reality (temperature, pressure, heating speed ...). Here we propose an enhanced ignition criterion which takes into account simplified chemical kinetics in decomposition reactions.

2 Numerical Aspects

We recall briefly some aspects that have been already detailed in previous works [3]. Our study is focused on the two-phase flow model developed by Gough [1], although other models can be found such as those reviewed in the book of Gidaspow [4]. This model takes into account the conservation of mass and momentum for the two phases and the conservation of energy for the gas phase. In addition to these partial differential equations, two transport equations for the enthalpy and the burnt thickness of the powder are added. The model used is a one-pressure model, because there is a relationship between the pressures of each phase. This kind of model is generally non hyperbolic and has already been studied [5].

To overcome this difficulty, we follow the idea presented in Ref. [5] and use a fractional step method. The convective part is split into two hyperbolic parts solved iteratively, while the source terms are solved at the third step. More details on the hyperbolicity are available in Ref. [6].

The system of partial differential equations is solved with a finite volume method adapted to the nonconservative case,

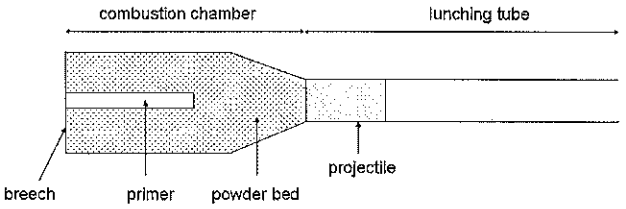

Fig. 1 Sketch of an initial configuration at firing

Manuscript received November 25, 2010; final manuscript received May 23, 2011; published online xx xx, xxxx. Assoc. Editor: Bo S. G. Janzon.

described in Ref. [7]. To calculate the numerical conservative flux, we choose to adapt the HLL scheme. In order to deal with the nonconservative terms, we follow the idea presented in Ref. [5] for a two-fluid model.

At the opposite, in the two-pressure models, the pressures are independent and the model is hyperbolic [8]. We propose such a two-pressure model in a slightly different approach, which consists in simulating the following relaxation model. This relaxation model is indeed very close to the Baer-Nunziato model [2]. In order to simplify the presentation, we present below the relaxation model in a one-dimensional framework. For further details, the reader is referred to [9].

The state variable is now

$$\nu W = (\alpha_2,\ \alpha_1\rho_1,\ \alpha_1\rho_1 u_1,\ \alpha_2\rho_2,\ \alpha_2\rho_2 u_2,\ \alpha_1 E_1,\ \alpha_2 E_2,\ d) \quad (1)$$

and the relaxation model is

$$\partial_t W + \frac{\partial F(W)}{\partial x} + C(W)\frac{\partial G(W)}{\partial x} = S(W). \quad (2)$$

The convective part corresponding to the last two terms on the left hand side is

$$\frac{\partial F(W)}{\partial x} + C(W)\frac{\partial G(W)}{\partial x} = \begin{pmatrix} u_2\dfrac{\partial \alpha_2}{\partial x} \\ \dfrac{\partial(\alpha_1\rho_1 u_1)}{\partial x} \\ \dfrac{\partial(\alpha_1(\rho_1 u_1^2 + p_1))}{\partial x} + p_1\dfrac{\partial \alpha_2}{\partial x} \\ \dfrac{\partial(\alpha_2\rho_2 u_2)}{\partial x} \\ \dfrac{\partial(\alpha_2(\rho_2 u_2^2 + p_2))}{\partial x} - p_1\dfrac{\partial \alpha_2}{\partial x} \\ \dfrac{\partial \alpha_1(E_1 + p_1)u_1}{\partial x} - p_1\dfrac{\partial \alpha_2}{\partial t} \\ \dfrac{\partial \alpha_2(E_2 + p_2)u_2}{\partial x} + p_1\dfrac{\partial \alpha_2}{\partial t} \\ u_2\dfrac{\partial d}{\partial x} \end{pmatrix} \quad (3)$$

where the total energy within phase k is $E_k = \rho_k\left(e_k + u_k^2/2\right)$. The source term is now

$$S(W) = \left(\Pi,\ \Gamma,\ D + w_I\Gamma,\ -\Gamma,\ -D - w_I\Gamma,\ \phi + w_I D + u_1 u_2\frac{\Gamma}{2},\ -\phi - w_I D - u_1 u_2\frac{\Gamma}{2},\ s_d\right) \quad (4)$$

where the velocity w_I denotes the average velocity:

$$w_I = \frac{u_1 + u_2}{2} \quad (5)$$

and where Γ, D, and ϕ respectively represent the interfacial mass transfer term, the drag effects and the interfacial heat exchange between the gas phase and the solid phase (see Refs. [3] and [9]). These are such that

$$D(u_2 - u_1) > 0 \quad \text{and also} \quad \phi(T_2 - T_1) > 0 \quad (6)$$

Assuming that μ_k stands for the chemical potential in phase k, the mass transfer term Γ is in agreement with the classical condition

$$\Gamma\left(\frac{\mu_2}{T_2} - \frac{\mu_1}{T_1}\right) > 0 \quad (7)$$

The source term now includes a contribution Π that governs the return towards a pressure equilibrium between the two phases, that is

$$\Pi = \frac{\alpha_1\alpha_2}{\tau_p}\frac{p_2 - p_1 - \Lambda(\alpha_2, \rho_2)}{p_2 + p_1 + \Lambda(\alpha_2, \rho_2)} \quad (8)$$

Formally, for very small values of the pressure relaxation time scale τ_P, we retrieve the closure law

$$p_2 = p_1 + \Lambda(\alpha_2, \rho_2) \quad (9)$$

The equation of state for the particulate phase $\rho_2(p_2, e_2)$ should be chosen in a suitable way. In practical applications, a stiffened gas EOS is used for the particulate phase.

Assuming that s_k denotes the specific entropy within phase k, it may be proved that the following entropy inequality governs variations of smooth solutions of the governing set of equations corresponding to the relaxation model

$$\frac{\partial}{\partial t}\left(\sum_{k=1,2}\alpha_k\rho_k s_k\right) + \frac{\partial}{\partial x}\left(\sum_{k=1,2}\alpha_k\rho_k s_k u_k\right) = \frac{\Pi}{T_2}(p_2 - p_1 - \Lambda) + \Gamma\left(\frac{\mu_2}{T_2} - \frac{\mu_1}{T_1}\right) + D(u_2 - u_1)\left(\frac{T_1 + T_2}{T_1 T_2}\right) + \frac{\phi}{T_2 T_1}(T_2 - T_1) \geq 0$$

The relaxation model always has real eigenvalues, and the associated right eigenvectors span the whole space provided that the relative velocity is not equal to c_k, which is very unlikely to happen in our applications.

Moreover, field by field jump conditions are unique. This is crucial since it means that these make sense; moreover, we may expect that stable approximations obtained with *different* schemes will converge towards a *unique* solution, even if shock waves occur in the solution. This has been examined in detail in Refs. [10,11].

We do not recall herein the basic numerical strategy, which is described in detail in Refs. [9] (see Ref. [12], also). Roughly speaking, this one is grounded on a *fractional step method that complies with the entropy inequality*, since it treats separately convective terms (first step) and source terms (second step). Exact or approximate Riemann solvers may be used within the first step that accounts for convective effects. Important details on the computation of the pressure relaxation step can be found in the latter reference (Ref. [9]). A crucial property of the second step of the algorithm is that it preserves the volumetric fractions α_k in the range [0,1]. Another advantage of the numerical method is that it enables to compute solutions with zero or nonzero values of the pressure relaxation time scale τ_P. The effect of a mesh refinement on approximations of two-fluid models has been extensively studied in Ref. [9] (see Refs. [10,11,13] too).

3 Physics of Ignition and Combustion

The ignition model takes a crucial role in the simulation of a complete ballistic cycle. The development of gas pressure waves and the compaction of the powder bed are indeed directly connected to front flame spreading. The numerical modeling of the ignition process is very difficult, due to the number of physical phenomena occurring (heat transfers in different way, chemical reactions...) in some milliseconds.

The most used ignition criterion is totally empirical: one considers that ignition occurs when the surface temperature of the grain reaches an experimentally determined temperature. However, this measured temperature is determined in very different conditions as in a combustion chamber. For example, the heat

transfer is only conductive and the temperature increase rate is only of the order of some Kelvin degrees per minutes. Once the grains are ignited, combustion phenomena occur. The most common combustion law was established by Vieille [14] and describes the combustion speed as a function of pressure. It is the case at high pressure, but at the beginning of the combustion, the temperature has also an influence on the combustion speed.

In this study, we propose a model which takes into account more physical processes in the different phases from the heating of the grains to the combustion at low pressure, with the constraint that the computing time has to remain as small as possible.

3.1 Heating of a Grain. We consider the one-dimensional configuration of the Fig. 2. The evolution of the temperature in the grain requires to solve the unsteady heat equation, to which we add a term corresponding to a chemical reaction in the solid phase, so

$$\rho_s c_s \frac{\partial T(z,t)}{\partial t} = \lambda_s \Delta T(z,t) + \omega_s(z,t) Q_{ex,s} \tag{11}$$

In the solid phase, the density is noted ρ_s, the specific heat c_s and the thermal conductivity λ_s. $T(z, t)$ is the temperature in the grain where z and t are respectively the space and time variables. The term $Q_{ex,s}$ corresponds to the chemical energy dissipated during combustion and $\omega_s(z, t)$ represents the reaction rate, considered neglected while the grain is not ignited.

The temperature at the initial time $t_0 = 0$ is uniform in the solid, so $T(z, 0) = T_0$, and the applied boundary conditions are $T(-\infty, t) = T_0$ and $T(0, t) = T_s(t)$. The grain is considered as a semi-infinite solid, but in practice we consider that the heating is so fast that the temperature remains constant in the grain's core. At the surface, the temperature $T_s(t)$ is unknown.

The energy balance applied to the solid in a fine thickness dz under the interface gives the relation

$$\frac{dE_s}{dt} = P_c + P_r \tag{12}$$

with E_s the energy of the elementary volume, P_c the chemical power generated through the combustion and P_r the received power. We can write

$$\frac{dE_s}{dt} = \rho_s c_s V \frac{\partial T}{\partial t} \tag{13}$$

$$P_c = 0 \tag{14}$$

$$P_r = A_{ext}\, \phi_e(t) - A_{int}\, \lambda_s \frac{\partial T}{\partial z} \tag{15}$$

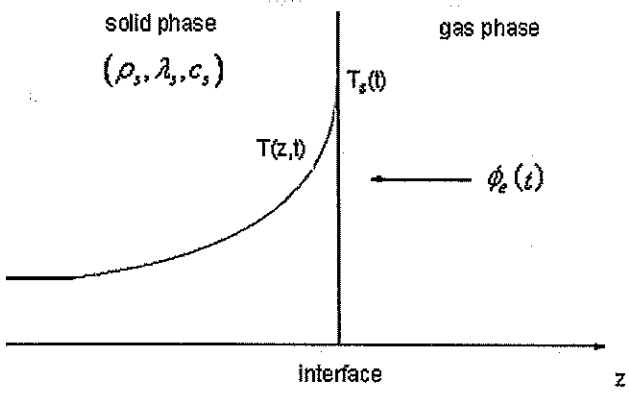

Fig. 2 1-D configuration at interface between solid and gas during heating

with V, A_{ext} and A_{int} respectively the volume, the external and internal surface of the considered thickness. If dz tends to zero, Eq. (12) gives the simpler relation

$$-\lambda_s \frac{\partial T}{\partial z} + \phi_e(t) = 0 \tag{16}$$

By defining the external flux $\phi_e(t)$ as a function of gas and solid surface temperature such as

$$\phi_e(t) = h_t(t)\left(T_g(t) - T_s(t)\right) \tag{17}$$

where $h_t(t)$ is the thermal exchange coefficient per surface unit (empirically determined) and $T_g(t)$ the known gas temperature, we can then compute the surface temperature $T_s(t)$.

The set of equations can be solved by a finite different method, but the computing time is too expensive. To get round this difficulty, we choose to approximate the temperature profile in the solid by a polynomial, such as in Ref. [15] with a 2nd order polynomial, in Ref. [16] with a 3rd order polynomial, eventually associated to an integral method [17]. Details on equation developments are available in Ref. [6].

Here we consider that the profile can be approximated by a piecewise function of the form

$$T(z,t) = \begin{cases} T_0 + B(t)\,(\delta + z)^p & \text{if} \quad -\delta \le z \le 0, \\ T_0 & \text{if} \quad z < \delta, \end{cases} \tag{18}$$

where p is the order of the polynomial. The function of time $B(t)$ and the depth of penetration of the thermal wave $\delta(t)$ remain inexplicit during the developments. Finally, we can express the surface temperature as

$$T_s(t) = T_0 + \sqrt{\frac{p+1}{p}\frac{\phi_e(t)\, Q_s(t)}{\lambda_s \rho_s c_s}} \tag{19}$$

where $Q_s(t)$ is the total absorbed energy computed by

$$\frac{dQ_s(t)}{dt} = \phi_e(t) \tag{20}$$

In order to validate the Eq. (19), different simulations have been made and results have been compared to the reference solution computed with a finite difference algorithm. Results showed that the order of the polynomial has to be greater or equal to four to obtain the best agreements between the methods [6].

3.2 Ignition Phase. Most of the interior ballistics codes consider that ignition occurs when the surface temperature reaches an experimentally determined ignition temperature. But it has been proved [18] that the ignition temperature is not constant and strongly depends on the heat flux received.

In order to obtain an ignition criterion that takes into account this dependence, we adapt the work of Ref. [18] to our case. Assuming that the solid decomposition is described by a 0th order reaction (hypothesis justified in Ref. [19]), the reaction rate can be written

$$\omega_s(z,t) = A_s \rho_s \exp\left(-\frac{E_s}{R_u T(z,t)}\right) \tag{21}$$

with A_s the preexponential factor, E_s the activation energy and R_u the universal constant of gas. Let us consider now the complete Eq. (11). When the solid approaches the ignition point, the reaction rate increases rapidly, and thus, the energy release due to the combustion, negligible during the heating phase, becomes suddenly important. The idea is to compare, on a reaction thickness

$z_r(t)$, the unsteady term, which represents the energy brought by the external heat flux, the energy release due to the decomposition reaction expressed by

$$\omega_s(z, t)\, Q_{ex,s} = A_s\, Q_{ex,s}\, \rho_s\, \exp\left(-\frac{E_s}{R_u\, T(z, t)}\right) \tag{22}$$

To evaluate the reaction thickness, we consider that its interior limit is reached when the reaction rate becomes negligible compared with the reaction rate at the surface, giving

$$\frac{\omega_s(z_r(t), t)}{\omega_s(0, t)} = \frac{1}{10} \tag{23}$$

where the fraction $(1/10)$ is chosen according to Ref. [18]. The temperature at the interior boundary of the reaction thickness is then

$$T_{boundary}(t) = \frac{E_s\, T_s(t)}{E_s + R_u\, T_s(t)\, \ln(10)}. \tag{24}$$

To compute numerically $z_r(t)$ with this last equation, we need to know the temperature profile in the solid. In the previous section, we used a piecewise polynomial function given by Eq. (18) to compute the surface temperature by Eq. (19). However, $B(t)$ and δ are not explicitly determined, so the temperature profile remains unknown.

We choose to describe the temperature profile with the help of an exponential function, defined, continuous and differentiable on the whole thickness of the grain, which takes the general form

$$T(z, t) = a(t) + b(t)\, \exp\left(\frac{z}{c(t)}\right) \tag{25}$$

The functions of time $a(t)$, $b(t)$, $c(t)$ are unknown. The boundary conditions, respectively applied to the radius r_e of a grain and to the surface, give the following two equations

$$a(t) + b(t)\, \exp\left(-\frac{r_e}{c(t)}\right) = T_0 \tag{26}$$

$$a(t) + b(t) = T_s(t) \tag{27}$$

but a third equation is needed to close the system. Two approaches can be considered:

(1) the temperature gradient at the surface can be approximated by a Robin condition

$$\lambda_s \left.\frac{\partial T(z, t)}{\partial z}\right|_{z=0^-} = \phi_e(t) \tag{28}$$

(2) the absorbed energy $Q_s(t)$, given by Eq. (20), can either be expressed by

$$Q_s = \int_{-r_e}^{0} \rho_s\, c_s\, (T(z, t) - T_0)\, dz \tag{29}$$

In both cases, a simple Newton method applied to the Eqs. (26), (27) and (28) or (29) can compute the three unknowns, and the temperature profile is then known. Results are similar for both approaches [6].

As an ignition criterion, we consider that ignition occurs when the energy released by the exothermal reaction becomes non negligible compared with the energy absorbed by the solid from the heat flux. This can be written

Table 1 Physical data for nitrocellulose

ρ_s	1.6×10^6 g.m^{-3}
c_s	1.67 J.g^{-1}.K^{-1}
λ_s	21.35×10^{-2} J.m^{-1}.s^{-1}.K^{-1}
E_s	167.5 kJ.mol^{-1}
A_s	10^{17} s^{-1}
$Q_{ex,s}$	251.2 J.g^{-1}
r_e	5.715×10^{-3} m
T_0	300 K

$$\int_0^{z_r(t)} \rho_s\, Q_{ex,s}\, A_s\, \exp(-E_s/R_u\, T(z, t))\, dz \geq \varepsilon \int_0^{z_r(t)} \rho_s\, c_s\, \frac{\partial T(z, t)}{\partial t}\, dz \tag{30}$$

where ε is a coefficient that depends on the energetic material. For the composite propellants, $\varepsilon = 0.15$ has been experimentally determined [18]. This data will be used in the following simulations but complementary simulations have shown that the value $\varepsilon = 0.3$ instead of $\varepsilon = 0.15$ conduct to a difference of only a few percent between the results. This can be explained by the sudden increase of the temperature caused by the exponential function in the neighborhood of the ignition point.

In order to validate our method, we simulate some experiments from several scientific teams synthesized in Ref. [18]. A nitrocellulose grain is heated with a laser beam of different constant intensities. Material data used for the nitrocellulose are listed in Table 1.

The results of simulations were presented in Ref. [20] and remembered in Table 2.

We want to catch the reader's attention on the fact that in these experiments, the thermal transfer is only radiative, whereas in interior ballistics problems, the heat transfer is mainly convective. Nevertheless, our model was built in a general case, without assumptions on the heat transfer.

Good agreement can be observed between the calculated and measured ignition delays and temperatures. The method can reproduce the variation of ignition temperature in function of the external heat flux intensity by taking into account a simple 0^{th} order decomposition reaction. Computing time remains low and it can be implemented in the three-dimensional code.

3.3 Combustion at Low Pressure. The most used combustion law is attributed to Vieille [14] and reads

$$u_s = a_n\, p^n \tag{31}$$

where u_s is the combustion rate, p the gas pressure and (a_n, n) a couple of empirical constants. This law is established for a pressure range from about 30 MPa to 500 MPa. But during a combustion cycle, pressures can exceed these limits, especially at the beginning of the ballistic cycle, when the gas pressure is very low.

Table 2 Comparison of measured and computed values for ignition delays and temperatures

	Ignition delay (ms)		Ignition temperature (K)	
ϕ_e (kW.m^{-2})	Measured	Computed	Measured	Computed
4186.8	2.2	2.0	590	591
891.8	34	33	542	545
456.4	115	111	-	528
418.7	132	129	521	525
184.2	550	550	-	505
41.9	7600	7800	-	472

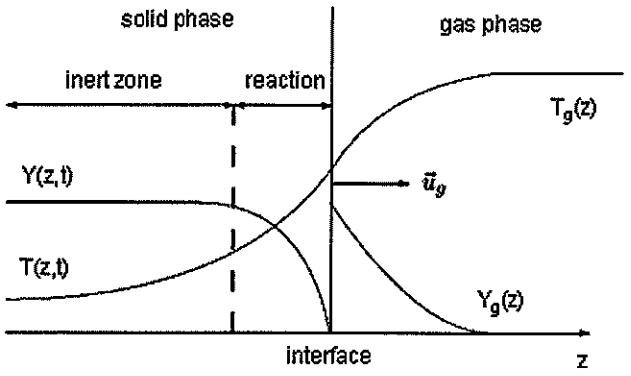

Fig. 3 1-D configuration at interface between solid and gas during combustion

In this case, the temperature has a great influence on the combustion velocity.

In this section, we propose a method to simulate the combustion at low pressure. In order to take into account the temperature in a model of low pressure combustion, we follow the idea of Weber et al. [21] and we couple the heat and transport equations of both phases, according to the one-dimensional configuration illustrated on Fig. 3.

During the combustion, the solid is decomposed in gas, so the interface will move from the right to the left. In order to simplify the calculations, the interface is supposed fixed at $z = 0$, that is why a mass flux that reads

$$m = \rho_s u_s = \rho_g u_g \tag{32}$$

has to be added to the equations. In the following notations, the subscript g corresponds to the gas phase whereas s corresponds to the solid phase. The equations for the solid phase are

$$\rho_s c_s \frac{\partial T(z,t)}{\partial t} + \rho_s c_s u_s \frac{\partial T(z,t)}{\partial z} = \lambda_s \frac{\partial^2 T(z,t)}{\partial z^2} + \omega_s Q_{ex,s} \tag{33}$$

$$\rho_s \frac{\partial Y(z,t)}{\partial t} + \rho_s u_s \frac{\partial Y(z,t)}{\partial z} = -\omega_s \tag{34}$$

with $z \leq 0$. We assume that a stationary premixed flame appears in the gas phase. The stationary behavior in the gas phase is justified in Ref. [22]. The equations for the solid phase become

$$\lambda_g \frac{d^2 T_g(z)}{dz^2} - \rho_g c_g u_g \frac{dT_g(z)}{dz} = -\omega_g Q_{ex,g} \tag{35}$$

$$\frac{\lambda_g}{c_g \,\mathrm{Le}} \frac{d^2 Y_g(z)}{dz^2} - \rho_g u_g \frac{dY_g(z)}{dz} = \omega_g \tag{36}$$

for $z \geq 0$. The Lewis number Le is considered equal to 1, according to Ref. [23]. We assume that the decomposition reactions are unimolecular

$$R(s) \xrightarrow{k_s} R(g) \xrightarrow{k_g} M(g) \tag{37}$$

where $R(s)$ is the reactive species in solid state, $R(g)$ the reactive species in gas state and $M(g)$ the inert product of the reaction, and the associated reaction constants are described by an Arrhenius law of the form

$$k_s = A_s \exp\left(-\frac{E_s}{R_u T}\right), \; k_g = A_g \exp\left(-\frac{E_g}{R_u T_g}\right) \tag{38}$$

The associated production rates read

$$\omega_s = \rho_s Y^{\tau_s} k_s, \; \omega_g = Y_g p^{\tau_g} k_g \tag{39}$$

where τ_k represents the order of the reaction in phase k. In the solid, the unimolecular reactions are generally considered as 1st order [24], but the abrupt profile of $Y(z, t)$ enables us to make the classical assumption of a 0th order reaction [19]. For the gas phase, we assume that the reaction is 2nd order [25].

The boundary conditions applied to the solid are

$$T(-\infty, t) = T_0, \; T(0^-, t) = T_s(t), \; Y(-\infty, t) = 1, \; Y(0^-, t) = 0. \tag{40}$$

For the gas phase, we introduce T_∞ as the flame temperature and $T_{s,g}(t)$ the temperature at the surface, on the gas phase side. We write

$$T_g(+\infty, t) = T_\infty, T_g(0^+, t) = T_{s,g}(t), Y_g(+\infty, t) = 0, Y_g(0^+, t) = 1. \tag{41}$$

At the interface, the mass balance equation gives

$$\rho_s u_s = \rho_g u_g = m \tag{42}$$

As we consider that all the solid-to-gas decomposed species are reactive, the species balance equation writes

$$m = m Y_g\big|_{0^+} - \frac{\lambda_g}{c_{p,g}} \frac{dY_g}{dz}\bigg|_{0^+} \tag{43}$$

The continuity of the temperature at the interface gives

$$T(0^-, t) = T_g(0^+, t), \tag{44}$$

and the energy balance applied to an elementary volume V in the solid under the surface (of external surface A_{ext} and internal surface A_{int}) has to take into account the heat flux from the flame, so we can write

$$\rho_s c_s V \frac{\partial T(z,t)}{\partial t} = A_{ext}\big(\Lambda_g + \phi_e(t)\big) + A_{int}\,\Lambda_s \tag{45}$$

with

$$\Lambda_s = \lambda_s \left|\frac{\partial T(z,t)}{\partial z}\right|_{z=0^-}, \quad \Lambda_g = \lambda_g \left|\frac{\partial T_g(z)}{\partial z}\right|_{z=0^+} \tag{46}$$

Finally, we consider that the specific heats are equal $c_s = c_g = c_p$ and we use a thick flame model [26] to describe the gas phase. According to Ref. [27], the activation energy in the gas phase is considered equal to zero

$$E_g = 0 \tag{47}$$

After some developments (detailed in Ref. [6]), the final algorithm takes the form

(1) compute the mass flux

$$m \frac{\partial Y(z,t)}{\partial z}\bigg|_{z=0^-} = -\omega_s(t) \tag{48}$$

(2) compute the intermediate value

$$a' = \frac{m c_g + \sqrt{m^2 c_g^2 + 4 \lambda_g A_g c_g p^2}}{2 \lambda_g} \tag{49}$$

(3) compute the temperature gradient in the gas phase

$$\Lambda_g = m Q_{ex,g}\left(1 - \frac{m c_g}{\lambda_g a'}\right) \tag{50}$$

Table 3 Solid data used in simulations

ρ_s	$1.6 \times 10^6\,\mathrm{g.m^{-3}}$	A_g	$2.36 \times 10^{-5}\,\mathrm{g.m^{-3}.s^{-1}.Pa^{-2}}$
c_p	$1.26\,\mathrm{J.g^{-1}.K^{-1}}$	E_g	$0\,\mathrm{J.mol^{-1}}$
λ_s	$16.08 \times 10^{-2}\,\mathrm{J.m^{-1}.s^{-1}.K^{-1}}$	$Q_{ex,g}$	$2336.23\,\mathrm{J.g^{-1}}$
A_s	$10^{17}\,\mathrm{s^{-1}}$	M_g	$24\,\mathrm{g.mol^{-1}}$
E_s	$168.57\,\mathrm{J.mol^{-1}}$	p	$10^7\,\mathrm{Pa}$
$Q_{ex,s}$	$175.85\,\mathrm{J.g^{-1}}$	r_e	5.715 mm
λ_g	$8.37 \times 10^{-4}\,\mathrm{J.m^{-1}.s^{-1}.K^{-1}}$	T_0	300 K

(4) compute the surface temperature with Eq. (45)
(5) compute the flame temperature

$$T_\infty(t) = T_s(t) + \frac{m\,Q_{ex,g}}{k_g\,c_g\,p^2}\left(a' - \frac{m\,c_g}{\lambda_g}\right) \tag{51}$$

(6) compute the new profiles $Y(z, t)$ and $T(z, t)$ in the solid phase

In this algorithm, it is necessary to compute the last step with a finite difference method, because the approximation made in the last section with an exponential function did not take into account the terms with mass flux in Eq. (33). Progresses to reduce computing time are needed.

It is difficult to validate this model because of the lack of data, particularly for the preexponential factors and the activation energies. Determination of these input parameters for some propellants is in progress. Up to now, we can only make a qualitative validation with data found in the literature [28], which are remembered in Table 3.

For this purpose, we simulate first the heating of a grain by an ignition flux of $4180\,\mathrm{kW.m^{-2}}$ at a constant gas pressure of 100 MPa. Ignition occurs after 1.43 ms for a surface temperature of 607 K. The combustion rate and the surface temperature converge towards a steady state, as illustrated in Fig. 4. This behavior is coherent with experimental observations. In this case, the final combustion rate and surface temperatures are respectively about 19.5 mm/s and 703 K. Experimental results are in progress.

We want now to study the system when the ignition flux is turned off at different moment. Three simulations are performed and results are illustrated in Fig. 5. Combustion without external heat flux, also called self-sustained combustion, is established at about 1.506 ms. Before, the surface temperature and the combustion speed decrease to zero whereas after this moment, they converge toward a steady state. This steady state is independent of the extinction time. As ignition time, the ignition criterion has previously given 1.43 ms. The combustion process needs a delay to establish a flame and thus an heat flux that continues the process without external heating.

The last qualitative validation we want to perform is to check the compatibility of the model with the Vieille's law. Simulations with constant gas pressure between 0.1 MPa and 170 MPa (an averaged lower limit of the domain of validity of the classical burning law) are executed and final steady combustion rates are recorded. On the log-log graph of Fig. 6, one can observe that the curve illustrating the combustion speed in function of pressure can be extrapolated by a straight line (in green) that corresponds to Eq. (31) with the parameters $a_n = 1.445 \times 10^{-9}$ SI and $n = 0.89$, which are in the range of classical values. Unfortunately, no data for this reactive material is available for the moment to confirm this result.

To summarize, we have first presented a method to describe the ignition of a propellant with a simple algorithm which takes into account a simple reaction in the solid phase and which can be easily implemented in a ballistic code. Then, we extended the study to the combustion at low pressure by introducing a simple reaction in the gas phase. For this part, a qualitative validation has been performed but the lack of data on chemical kinetics does not allow us to proceed to a rigorous validation. However, the algorithm gives results in good agreement with experimental observations but can unfortunately not yet be adapted to the ballistic code due to the increase of computing time by the use of a finite difference method.

4 Experimental Validation

In this section some numerical simulations of ballistic cycles will be presented. The first two test cases were used as benchmark for interior ballistics code. Studied guns are the virtual AGARD 132 mm gun [29] and the 40 mm gun [30]. Some results have been already previously presented in Ref. [7] but are completed with new ones. The data for both cases are synthesized in [6].

4.1 Agard 132 mm. The results of the benchmark presented in Ref. [29] show a high dispersion. The extreme values are reported in Table 4 and we will refer to them as "reference results."

Here we study the case where the primer is simulated. Two configurations are considered and illustrated in Fig. 7. For each configuration, the primer works during 10 ms and the source terms corresponding to the primer are $\Gamma_{ign} = 13132\,\mathrm{kg.m^{-3}.s^{-1}}$ and $Q_{ign} = 1.5702 \times 10^6\,\mathrm{J.kg^{-1}}$.

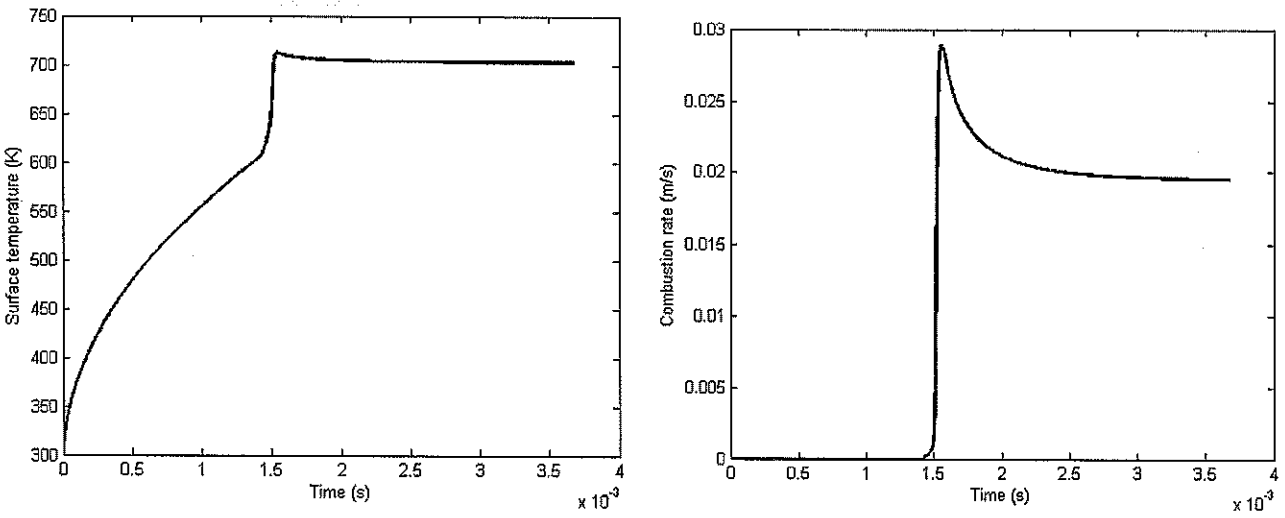

Fig. 4 Evolution of surface temperature and combustion rate with a constant heat flux

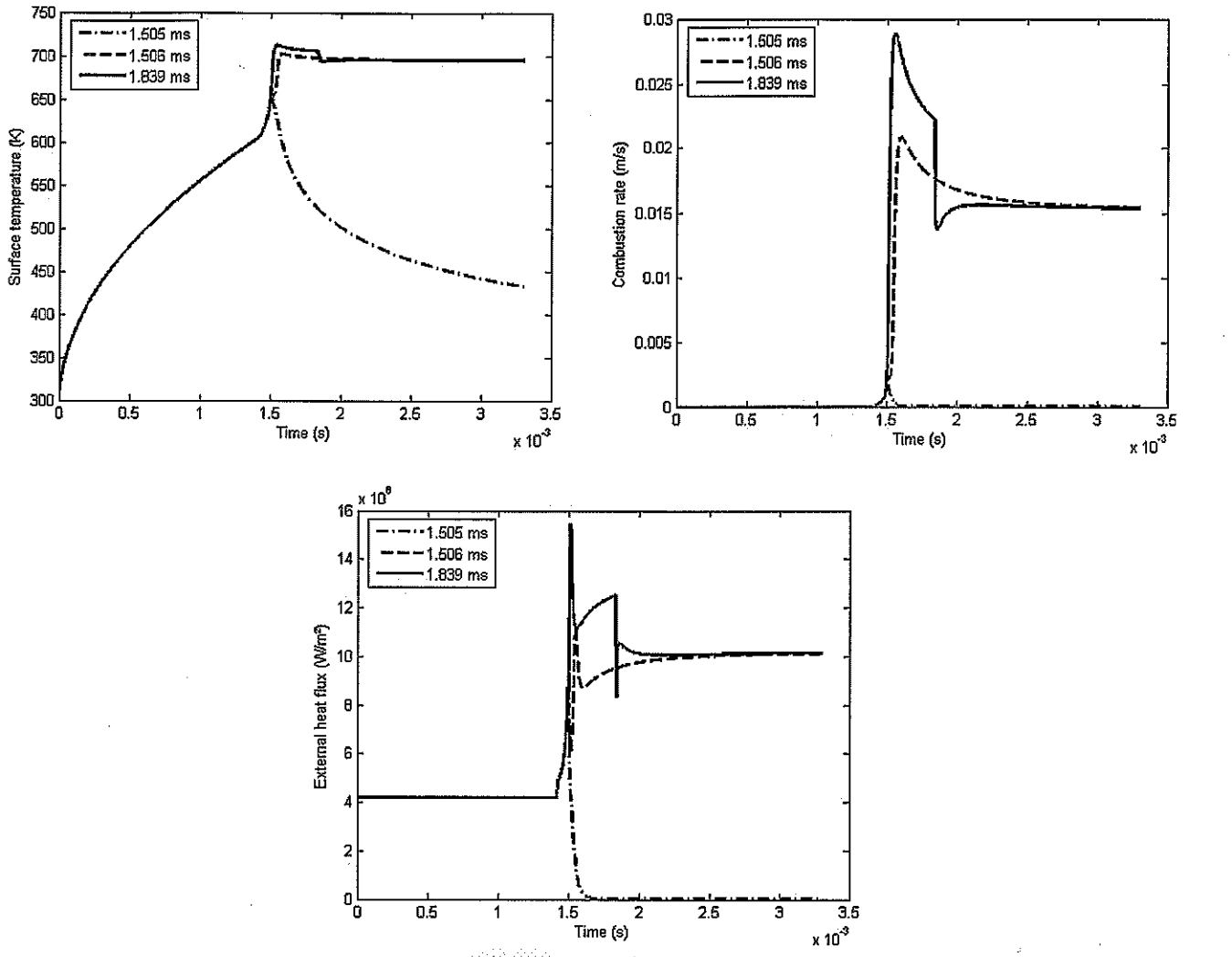

Fig. 5 Evolution of surface temperature, combustion rate and total external heat flux when the ignition flux is suddenly switched off

The results for the configuration 1 are reported in Table 5. The maximal pressures are always near the highest values of the reference results, but remain coherent. The difference between the 1D and 2D simulations can be explained by the modeling of the primer: the flow per unit of volume Γ_{ign} is the same in all cases, so the mass addition in the 2D simulations is lower than in the 1D simulations. The powder bed ignition is thus more diffused, making the pressure evolution slower and smoother. For the 1D case, the refinement of the mesh increases the accuracy of the scheme, making the pressure peaks sharper. On a two-dimensional mesh, refining the mesh smooths the pressure waves according to the previous remark on Γ_{ign}. This source term has to be corrected in order to obtain primer conditions independent of the mesh used.

The configuration 2 is more realistic. The primer is modeled by source terms in five points at z = 0 mm, z = 31.75 mm, z = 63.5 mm, z = 95.24 mm and z = 127 mm. The results are synthesized in Table 6 and Table 7. They correspond to the reference results, excepted with the ignition times. As for the previous configuration, the primer modeling depends on the mesh size. The finer the grid is, the less power and mass the primer produces.

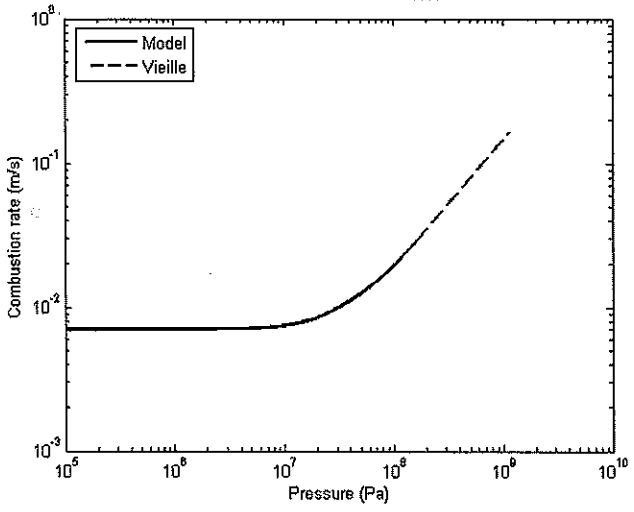

Fig. 6 Steady combustion rate in function of pressure: compatibility with classical burning law

Table 4 Results of the benchmark on the Agard gun

Computed data	Results (1D simulation)	Results (2D simulation)
Max. shot base pressure (MPa)	324 – 390	328 – 368
Max. breech pressure (MPa)	350 – 423	360 – 396
Muzzle velocity (m/s)	660 – 722	687 – 711
Exit time (ms)	14.36 – 16.58	15.06 – 16.85

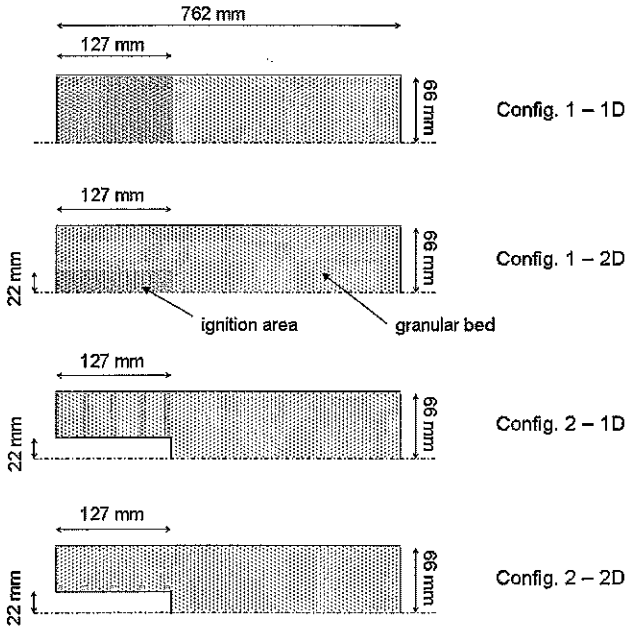

Fig. 7 Configuration in the combustion chamber at initial time

4.2 40 mm Gun. In this section, the 40 mm gun is studied. In this gun, the cross section is now variable (42 mm diameter at breech and 40 mm diameter at muzzle). The primer has two holes at $z = 10$ mm and $z = 35$ mm. The powder used is of the type triple base, meaning that it is composed of three chemical species. Here again, no chemical data is available to use our ignition model. We consider then that ignition occurs when the surface temperature reaches 444 K.

Experimental results have been used in Ref. [30] to compare the simulations of different ballistic codes. For a mass of powder of 440 g and a projectile mass of 790 g, the maximal pressure recorded is 428 MPa and the muzzle velocity is 1234 m/s. In many cases, the benchmark data had to be corrected in order to fit the calculated results to the measured ones. The vivacity and the chemical energy of the powder were the most modified values.

Here, we build a "zero-dimensional model" to simulate the primer, based on the Gough equations. This means that we simulate the evolution of the conditions in the primer with the assumption that these conditions are the same in the whole volume of the primer. The model is described by the following four differential equations

$$\begin{aligned}
&\frac{d}{dt}\alpha_2^* = -\frac{\Gamma_{comb}^*}{\rho_2^*}\\
&\frac{d}{dt}\left(\alpha_1^*\rho_1^*\right) = \Gamma_{comb}^*\\
&\frac{d}{dt}\left(\alpha_1^*\rho_1^* e_1^*\right) = \Gamma_{comb}^*\left(Q_{ex}^* + \frac{p_1^*}{\rho_1^*}\right)\\
&\frac{d}{dt}d^* = \dot{r}^*
\end{aligned} \tag{52}$$

Table 5 Effect of mesh size on 1D and 2D results for Agard gun – configuration 1

Computed data	500 cells	1000 cells	2000 cells	500X5 cells	500X10 cells
Max. shot base pressure (MPa)	388	389	391	366	365
Max. breech pressure (MPa)	423	421	421	402	400
Muzzle velocity (m/s)	707	712	716	695	694
Exit time (ms)	14.56	14.58	14.60	16.25	16.69

Table 6 Effect of mesh size on 1D results for Agard gun – ignition in five points

Computed data	500 cells	1000 cells	2000 cells
Max. shot base pressure (MPa)	372	364	362
Max. breech pressure (MPa)	408	400	397
Muzzle velocity (m/s)	698	699	703
Exit time (ms)	15.46	16.19	16.83

Table 7 Effect of mesh size on 2D results for Agard gun – ignition in 5 points

Computed data	500X1 cells	500X5 cells	500X10 cells
Max. shot base pressure (MPa)	354	356	362
Max. breech pressure (MPa)	388	391	398
Muzzle velocity (m/s)	688	695	693
Exit time (ms)	15.47	15.42	21.78

corresponding to the balance equations of gas mass, powder mass, gas energy and burnt thickness. The superscript * corresponds to the state in the primer. The term Γ_{comb} represents the production of gas through the combustion. The combustion rate $\dot{r}$ follows a Vieille's law.

The primer is 50 mm-length and 10 mm-diameter, with two holes at z = 10 mm and z = 35 mm. It is filled with 4.15 g of black powder with the characteristics

- grains: sphere with 1.77 mm-diameter
- density: 1700 kg/m^3
- chemical energy: 1.3045 MJ/kg

Since we do not have all the data required for a simulation, we have to make some complementary hypothesis:

- the coefficients of the combustion rate equation are the same as for the propellant
- the gas produced by the combustion of the black powder have the same thermodynamical properties as the gas produced in the combustion chamber

The same two values as in the perfect ignition case for the chemical energy of the propellant were used: $Q_{ex,1} = 5.071$ MJ/kg and $Q_{ex,2} = 5.471$ MJ/kg. The simulations on 1D and 2D meshes are exposed in Table 8.

The numerical results are in agreement with the reference results, except for the exit time that is much greater in the 1D simulations. As for the previous cases, this problem comes from the construction of the mesh, and this has to be solved in the future. It is to notice that the muzzle velocity is generally underestimated in comparison with the other codes. No explanation is available for the moment. We can observe that the pressure at the breech is higher on a one-dimensional mesh whereas the pressure at the shot base is lower. The difference between the pressures on both sides of the computing domain is then greater in the 1D case.

Table 8 Results for the 40 mm gun on 1D and 2D meshes – primer simulated

	500 × 1 grid		500 × 5 grid	
Computed data	$Q_{ex,1}$	$Q_{ex,2}$	$Q_{ex,1}$	$Q_{ex,2}$
Max. shot base pressure (MPa)	325	377	341	400
Max. breech pressure (MPa)	444	519	434	504
Muzzle velocity (m/s)	1169	1237	1148	1214
Exit time (ms)	27.39	26.85	9.97	9.50

5 Conclusion and Future Work

We have developed a two-phase flow code applied to interior ballistic problems. Its main features are the possibility to simulate multidimensional problems and the implementation of an advanced ignition criterion. The set of partial differential equations describing the flows is not always hyperbolic and contains nonconservative terms, so we had to adapt a finite volume method to handle these characteristics. Works on different approaches such as a relaxation method are in progress.

On a physical point of view, we built a model which takes into account simplified chemical reactions in both phases (gas and solid) to obtain more realistic ignition temperatures and delays. Optimized algorithms were developed to limit the computing time increase. Some experiments are still required to complete the validation.

The comparisons of simulations with other ballistic codes and experimental results showed that we obtain results in good agreement on one- and two-dimensional meshes. Unfortunately, the lack of physical data did not enable us to use our advanced ignition criterion, so the physical models used were similar to the other codes.

An interesting way to improve the results is to make the simulation of the primer independent of the mesh, which is not yet the case, as some results demonstrated. A second perspective is the use of nonhomogeneous meshes to increase the accuracy and the computing time of the code, by refining the grid in the neighborhood of the primer surface and using a coarse mesh in the lunching tube.

References

[1] Gough, P. S., 1979, "Modeling of Two-Phase Flows in Guns," AIAA J. **66**, pp. 176–196.

[2] Baer, M. R. and Nunziato, J. W., 1986, "A Two-Phase Mixture Theory for the Deflagration to Detonation (DDT) Transition in Reactive Granular Materials," International Journal on Multiphase Flow, **12**(6), pp. 861–889.

[3] Nussbaum, J., Helluy, Ph., Hérard, J.-M., and Carrière, A., 2006, "Numerical Simulations of Gas-Particle Flows with Combustion," Journal of Flow, Turbulence and Combustion, **76**(4), pp. 403–417.

[4] Gidaspow, D., 1994, *Multiphase Flow and Fluidization*, Academic, London, UK.

[5] L. Combe, and Hérard, J.-M., 1999, "Finite Volume Algorithm to Compute Dense Compressible Gas-Solid Flows," AIAA J. **37**(3), pp. 337–345.

[6] Nussbaum, J., 2007, "Modélisation et Simulation Numérique d'un Ecoulement Diphasique de la Balistique Intérieure," Ph.D. thesis, University of Strasbourg/ French-German Research Institute of Saint-Louis, France.

[7] Nussbaum, J., Helluy, Ph., Hérard, J.-M., and Carrière, A., 2007, "Numerical Simulations of Reactive Two-Phase Gas-Particle Flows," *39th AIAA Thermophysics Conference*, AIAA Paper No. 2007-4161, Miami, USA.

[8] Kapila, A. K., Son, S. F., Bdzil, J. B., Menikoff, R., and Stewart, D.S., 1997, "Two-Phase Modeling of DDT: Structure of the Velocity-Relaxation Zone," Phys. Fluids, **9**(12), pp. 3885–3897.

[9] Gallouët, T., Helluy, Ph., Hérard, J.-M., and Nussbaum, J., 2010, "Hyperbolic Relaxation Model for Granular Flow," M2AN, **44**(2), pp. 371–400.

[10] Hérard, J.-M. and Hurisse, O., 2005, "A Simple Method to Compute Standard Two-Fluid Models," Int. J. Comput. Fluid Dyn. **19**(7), pp. 475–482.

[11] Guillemaud, V., 2007, "Modélisation et Simulation Numérique des Ecoulements Diphasiques par une Approche Bifluide à Deux Pressions," Ph.D. thesis, University of Aix Marseille I, France.

[12] Gallouët, T., Hérard, J.-M., and Seguin N., 2004, "Numerical Modelling of Two-Phase Flow Using the Two-Fluid Two-Pressure Approach," M3AS, **14**(5), pp. 663–700.

[13] Girault, L., and Hérard, J.-M., 2010, "A Two-Fluid Model in a Porous Medium," M2AN, **44**(6), pp. 1319–1348.

[14] Vieille, P., 1893, *Etude sur le Mode de Combustion des Substances Explosives.*

[15] Porterie, B., 1988, "Modélisation de la Phase d'Allumage d'une Charge Propulsive en Balistique Intérieure," Ph.D. thesis, University of Aix-Marseille I, France.

[16] Della Pieta, P. and Reynaud, C., 2000, "Numerical Investigations for Modeling Interior Ballistics Two-Phase Flow," *European Forum on Ballistics of Projectiles*, Saint-Louis, France.

[17] Peretz, A., Kuo, K. K., Caveny, L. H., and Summerfield, M., 1973, "Starting Transient of Solid-Propellant Rocket Motors with High Internal Gas Velocities," AIAA J. **11**(2), pp. 1719–1727.

[18] Lengellé, G., Bizot, A., Duterque, J., and Amiot, J. C., 1991, "Allumage des Propergols Solides," La Recherche Aérospatiale, **2**, pp. 1–20.

[19] Lengellé, G., 1970, "Thermal Degradation Kinetics and Surface Pyrolysis of Vinyl Polymers," AIAA J. **8**, pp. 1989–1998.

[20] Nussbaum, J., Franco, P., and Carrière, A., 2007, "Powder Ignition Modelling in Interior Ballistic Problem," *21st Int. Colloquium on the Dynamics of Explosives and Reactive Systems*, Poitiers, France.

[21] Weber, J. W., Brewster, M. Q., and Tang, K.C., 2005, "Radiative Ignition and Extinction Dynamics of Energetic Solids," J. Thermophys. Heat Transfer, **19**(3), pp. 257–265.

[22] Brewster, M. Q. and Son, S. F., 1995, "Quasi-Steady Combustion Modeling of Homogeneous Propellants," Combust. and Flame, **103**, pp. 11–26.

[23] Poinsot, T. and Veynante, D., 2005, *Theoretical and Numerical Combustion*, R.T. Edwards, ed., Philadelphia, PA.

[24] Warnatz, J., Maas, U., and Dibble, R. W., 2006, *Combustion – Physical and Chemical Fundamentals, Modeling and Simulation, Experiments, Pollutant Formation*, 4th ed., Springer-Verlag, Berlin.

[25] Ward, M. J., Son, S. F., and Brewster, M. Q., 1998, "Role of Gas- and Condensed-Phase Kinetics in Burning Rate Control of Energetic Solids," Combust. Theory Modell. **2**, pp. 293–312.

[26] Brewster, M. Q., Ward, M. J., and Son, S.F., 1997, "New Paradigm for Simplified Combustion Modeling of Energetics Solids: Branched Chain Gas Reaction," *33rd AIAA/ASME/SAE/ASEE Joint Propulsion Conference and Exhibit*, Seattle, WA, AIAA Paper No. 97-3333.

[27] Ward, M. J., Son, S. F., and Brewster, M. Q., 1997, "Steady Deflagration of HMX with Simple Kinetics: A New Modeling Paradigm," *35th AIAA Aerospace Sciences Meeting and Exhibit*, AIAA Paper No. 97–0590.

[28] Jackson, T. L., Massa, L., and Brewster, M. Q., 2004, "Unsteady Combustion Modelling of Energetic Solids, Revisited," Combust. Theory Modell. **8**, pp. 513–532.

[29] Woodley, C., Carrière, A., Franco, P., Gröger, T., Hensel, D., Nussbaum, J., Kelzenberg, S., and Longuet, B., 2005, "Comparisons of Internal Ballistics Simulations of the Agard Gun," *22nd International Symposium on Ballistics*, Vancouver, Canada.

[30] Woodley, C., Carrière, A., Franco, ■, Nussbaum, J., Chabaux, X., and Longuet, B., 2007, "Comparisons of Internal Ballistics Simulations of 40mm Gun Firings," 23rd *International Symposium on Ballistics*, Tarragona, Spain.